Fenestrations control resting-state block of a voltage-gated sodium channel

Tamer M. Gamal El-Din[a,1], Michael J. Lenaeus[a,b,1], Ning Zheng[a,c,2,3], and William A. Catterall[a,2,3]

[a]Department of Pharmacology, University of Washington, Seattle, WA 98195; [b]Division of General Internal Medicine, Department of Medicine, University of Washington, Seattle, WA 98195; and [c]Howard Hughes Medical Institute, University of Washington, Seattle, WA 98195

Contributed by William A. Catterall, October 31, 2018 (sent for review September 4, 2018; reviewed by Ryan Hibbs, Michael C. Sanguinetti, and Joerg Striessnig)

Potency of drug action is usually determined by binding to a specific receptor site on target proteins. In contrast to this conventional paradigm, we show here that potency of local anesthetics (LAs) and antiarrhythmic drugs (AADs) that block sodium channels is controlled by fenestrations that allow drug access to the receptor site directly from the membrane phase. Voltage-gated sodium channels initiate action potentials in nerve and cardiac muscle, where their hyperactivity causes pain and cardiac arrhythmia, respectively. LAs and AADs selectively block sodium channels in rapidly firing nerve and muscle cells to relieve these conditions. The structure of the ancestral bacterial sodium channel Na_VAb, which is also blocked by LAs and AADs, revealed fenestrations connecting the lipid phase of the membrane to the central cavity of the pore. We cocrystallized lidocaine and flecainide with Na_VAb, which revealed strong drug-dependent electron density in the central cavity of the pore. Mutation of the contact residue T206 greatly reduced drug potency, confirming this site as the receptor for LAs and AADs. Strikingly, mutations of the fenestration cap residue F203 changed fenestration size and had graded effects on resting-state block by flecainide, lidocaine, and benzocaine, the potencies of which were altered from 51- to 2.6-fold in order of their molecular size. These results show that conserved fenestrations in the pores of sodium channels are crucial pharmacologically and determine the level of resting-state block by widely used drugs. Fine-tuning drug access through fenestrations provides an unexpected avenue for structure-based design of ion-channel–blocking drugs.

voltage-gating | sodium channel | fenestration | antiarrhythmic drugs | local anesthetics

Voltage-gated sodium (Na_V) channels are responsible for generation of action potentials in electrically excitable cells (1). They encode and transmit information in the form of frequency-modulated electrical signals. These channels are composed of four identical subunits or four homologous domains (DI–DIV), each containing six transmembrane segments (S1–S6) (2, 3). The first four segments (S1–S4) constitute the voltage-sensing module, which detects changes in membrane potential and transduces them to the pore (2, 3). The S5 and S6 segments and the P-loop between them form the pore, which is opened by an iris-like motion of the activation gate at the intracellular ends of the S6 segments (2, 3).

Inherited or acquired dysfunction of Na_V channels causes chronic pain, cardiac arrhythmia, periodic paralysis, and epilepsy (4–7). Local anesthetics (LAs) and antiarrhythmic drugs (AADs) are used to prevent excessive electrical signaling by blocking Na_V channels during therapy of pain and cardiac arrhythmia (8, 9). Both types of drugs are thought to bind to a receptor site in the central cavity in the pore (1, 10–14). The complex therapeutic actions of these drugs derive from three interacting processes: slow resting-state block, rapid open-state block, and high-affinity inactivated-state block (15, 16). This state-dependent mode of block is crucial for clinical use of these drugs, as it allows them to selectively prevent generation of high-frequency action potentials characteristic of intense pain and cardiac arrhythmia, while having less effect on normal electrical signaling (8, 16). The Modulated Receptor Hypothesis posits that resting-state block is mediated by drug entry from the lipid phase of the membrane into the drug receptor site in the pore, and rapid open-state block occurs as the drug enters the open pore from the cytoplasm (15). Both of these forms of block are enhanced when the channel enters the inactivated state, which has high affinity for bound drug (15). It is well-established that LAs and AADs can reach their binding site from the intracellular side if the activation gate is open, which gives open-state block, and that inactivation increases the affinity for drug binding (15, 16). On the other hand, the hypothesis that direct access from the membrane phase causes resting-state block has lacked experimental support.

Ancestral bacterial sodium channels are blocked by LAs and AADs (17–20), and the structure of the bacterial sodium channel Na_VAb revealed fenestrations connecting the lipid phase of the membrane to the central cavity of the pore (21, 22), which are conserved in eukaryotic Na_V channels (23, 24) and are observed in potassium channels (25). The discovery of fenestrations in Na_VAb led to the hypothesis that they provide an access pathway for resting-state block (21, 23, 24). We have tested this hypothesis by defining the receptor site for LAs and AADs through X-ray crystallography, resetting the size of the fenestrations in Na_VAb

Significance

Voltage-gated sodium channels initiate electrical signals in nerve and cardiac muscle, where their hyperactivity causes pain and cardiac arrhythmia. Local anesthetics and antiarrhythmic drugs selectively block sodium channels in rapidly firing nerve and muscle cells to relieve these conditions. We studied an ancestral bacterial sodium channel to elucidate the structure of the drug-binding site and the pathway for drug entry to the receptor site. We found that the drug-binding site is located in the center of the transmembrane pore, through which sodium ions move and fenestrations form an access pathway for drug entry directly from the cell membrane. These results show how these widely used drugs block the sodium channel and have important implications for structure-based design of next-generation drugs.

Author contributions: T.M.G.E.-D., M.J.L., N.Z., and W.A.C. designed research; T.M.G.E.-D. and M.J.L. performed research; T.M.G.E.-D., M.J.L., and N.Z. analyzed data; and T.M.G.E.-D., M.J.L., and W.A.C. wrote the paper.

Reviewers: R.H., University of Texas Southwestern Medical Center; M.C.S., University of Utah; and J.S., University of Innsbruck.

The authors declare no conflict of interest.

Data deposition: The following data have been deposited in the Protein Data Bank (PDB), www.wwpdb.org: Na_VAb/I217C, F203A (PDB ID code 6MVV); Na_VAb/I217C, F203W (PDB ID code 6MVW); Na_VAb/1217C, complexed with flecainide (PDB ID code 6MVX); and Na_VAb/I217C, 1-226, crystallized in the presence of lidocaine (6MVY).

[1]T.M.G.E.-D. and M.J.L. contributed equally to this work.

[2]N.Z. and W.A.C. contributed equally to this work.

[3]To whom correspondence may be addressed. Email: nzheng@uw.edu or wcatt@uw.edu.

This article contains supporting information online at www.pnas.org/lookup/suppl/doi:10.1073/pnas.1814928115/-/DCSupplemental.

Published online December 5, 2018.

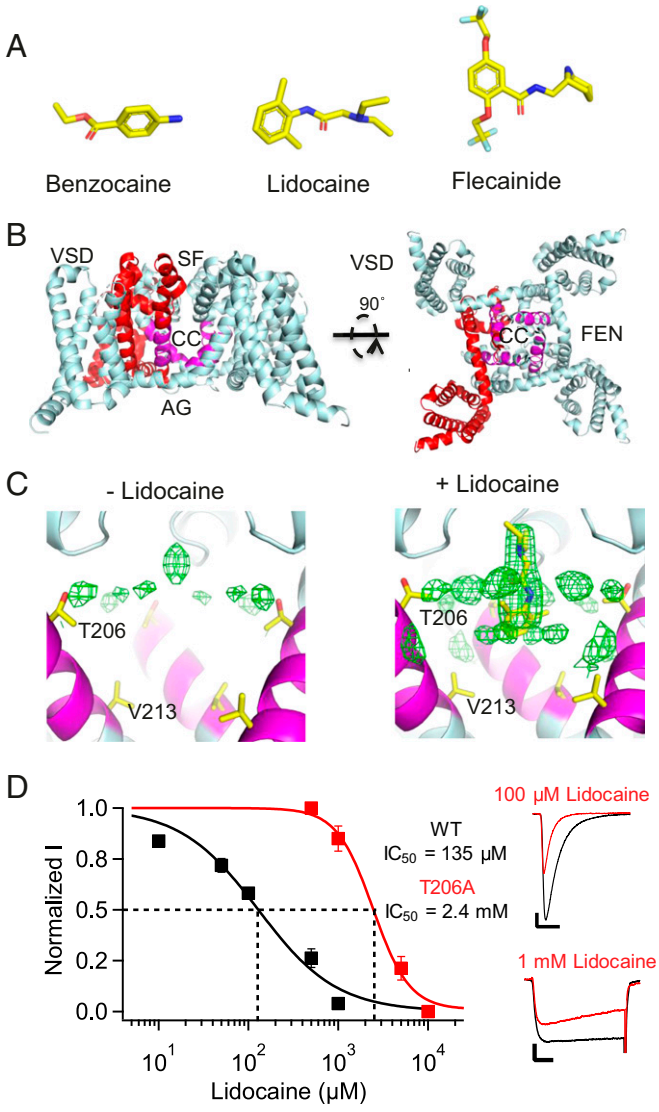

Fig. 1. Binding site for lidocaine on Na_VAb. (*A*) LA/AADs used in this study: benzocaine, lidocaine, and flecainide. (*B*) The structure of $Na_VAb/I217C/\Delta40$ is shown in cartoon format. Residues homologous to those shown to be involved in LA/AAD binding are highlighted in magenta, and channel regions are labeled as VSD (voltage sensor), SF (selectivity filter), CC (central cavity), AG (activation gate), and FEN (fenestration). (*C*, *Left*) The structure of $Na_VAb/I217C/\Delta40$ when solved without any drugs in solution. The protein model is shown in cartoon format with the LA/AAD-binding site highlighted in magenta and sidechains of key residues (T206, V213) shown in stick format. Fo-Fc electron density contoured at 3σ is shown as green mesh, as calculated from data deposited as Protein Data Bank ID code 5vb8. (*C*, *Right*) The structure of $Na_VAb/I217C/\Delta40$ when solved with lidocaine in solution. The protein and electron density are displayed as on the *Left*. Lidocaine was manually placed into this model. (*D*) Effect of mutation of T206 on resting-state block of Na_VAb by lidocaine. The peak current recorded during the first pulse after 2 min of drug perfusion was taken as a measure of drug inhibition of the resting state. (*Left*) Concentration-response curves for lidocaine inhibition of Na_VAb/WT (black, IC_{50} = 135 ± 20 μM), $Na_VAb/T206A$ (red, IC_{50} = 2.4 ± 0.3 mM) under conditions for resting-state block (*SI Appendix, SI Materials and Methods*). Each data point is an average of 5–10 cells. (*Right*) Sodium current recordings of Na_VAb/WT and $Na_VAb/T206A$ in the absence (black) and presence (red) of 100 μM and 1 mM lidocaine, respectively. Pulses were applied from holding potentials of −160 or −140 mV to 0 mV. The vertical and horizontal scale bars represent 0.2 nA and 10 ms, respectively.

through introduction of site-directed mutations, and analyzing the resulting effects on the potency for resting-state block by LAs and AADs of different molecular size by electrophysiology. We use the term "potency" to describe drug block quantitatively, rather than "affinity," because our results show that both drug access and drug-binding affinity contribute substantially to the concentration-dependent drug block that we measure.

Results

The Receptor Site for Lidocaine and Flecainide in Na_VAb. We solved crystal structures of Na_VAb in complex with the LA/AAD lidocaine (Fig. 1 *A*–*C* and *SI Appendix*, Table S1) and the AAD flecainide (Fig. 2 *A* and *B* and *SI Appendix*, Table S1), two of the most widely prescribed Na_V channel-blocking drugs. Complexes were prepared by mixing the drugs with purified Na_VAb protein before incorporation into bicelles, and cocrystals were formed in hanging drops as previously described for Na_VAb alone (21). Structures determined

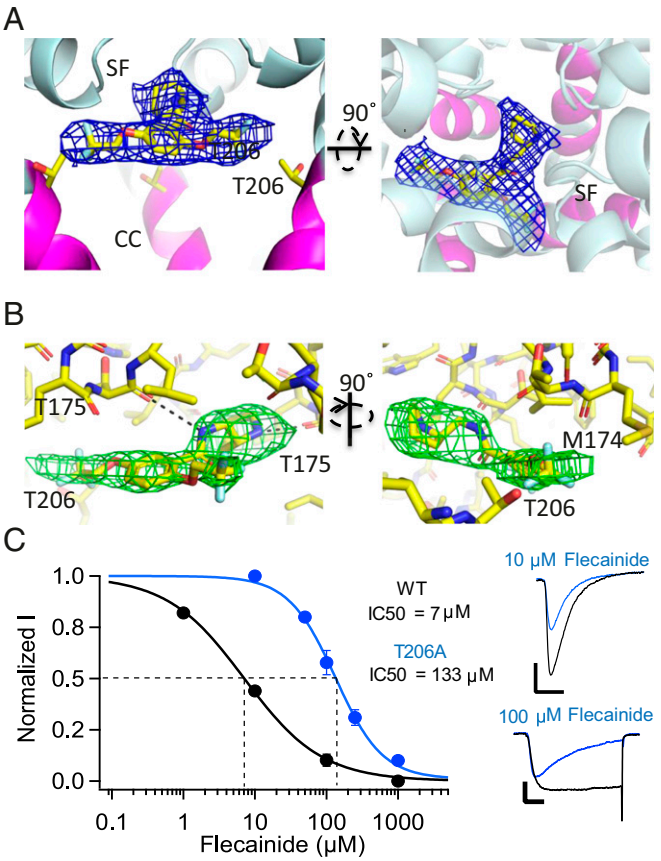

Fig. 2. Binding site for flecainide on Na_VAb. (*A*) Orthogonal views of flecainide in complex with $Na_VAb/I217C$. In each case the protein is displayed as cartoon helices, with the AAD binding site highlighted in magenta ribbon and sidechain sticks. Functional areas of the channel labeled as in Fig. 1. Flecainide is displayed as sticks, with yellow = carbon, red = oxygen, blue = nitrogen, and gray = fluoride. Electron density (2fo-fc) is displayed as a blue mesh, contoured at 1 σ. (*B*) Close-up, orthogonal views of flecainide in complex with $Na_VAb/I217C$. Flecainide and flecainide-associated residues are shown in stick format as in *A*, and potential hydrogen bonds are shown as black dashes. Omit map Fo-Fc electron density calculated from a model excluding flecainide is shown as a green mesh, contoured at 3 σ. (*C*) Effect of mutation of T206 on resting-state block of Na_VAb by flecainide. The peak current recorded during the first pulse after 2 min of drug perfusion was taken as a measure of drug inhibition of the resting state. (*Left*) Concentration-response curves for flecainide inhibition of Na_VAb/WT (black circles, IC_{50} = 7 ± 0.38 μM), $Na_VAb/T206A$ (blue circles, IC_{50} = 133 ± 6.5 μM). Each data point is an average of 5–10 cells. (*Right*) Sodium current recordings of Na_VAb/WT and $Na_VAb/T206A$ in the absence (black) and presence of 10 or 100 μM flecainide (blue) under conditions for resting-state block (*SI Appendix, SI Materials and Methods*). Pulses were applied from holding potentials of −160 or −140 mV to 0 mV. The vertical and horizontal scale bars represent 0.5 nA and 10 ms, respectively.

from crystals grown with lidocaine contained a large electron density peak in the central cavity of Na_VAb, which was not present when crystals were grown without drug (Fig. 1*C*). This peak is located on the intracellular side of the selectivity filter, adjacent to the positions of amino acid sidechains that are important for drug binding (10–14). Because Na_VAb has fourfold symmetry, the electron density is expected to reflect four equivalent binding poses of lidocaine (*SI Appendix*, *SI Discussion*). Our observed electron density is consistent with that expectation, with the tertiary amino group of lidocaine located on the pore axis and projecting upward toward the selectivity filter (Fig. 1*C*). Mutation of the closely interacting residue T206 to alanine reduced the potency of resting state block by 17.8-fold (Fig. 1*D*). This mutation also slowed inactivation and shifted the voltage dependence of Na_VAb gating (*SI Appendix*, *SI Discussion*). The reduced affinity for drug block with this mutant confirms placement of the bound lidocaine, but fourfold averaging of the electron density caused the amide linker and aromatic moiety of lidocaine to be represented in quadruplicate (Fig. 1*C*) and prevents us from determining all of the specific chemical interactions involved in drug binding.

Similar experiments with the AAD flecainide revealed electron density in a comparable location in the pore (Fig. 2*A*). Perhaps because flecainide is larger and more asymmetric, we observed a single binding pose for this drug with its tertiary amino group projecting upward into the selectivity filter and its fluoromethylated aromatic rings projecting farther toward the wall of the central cavity than we observed with lidocaine (Fig. 2*B*). As for lidocaine, mutation of T206 caused a major reduction in drug potency (18.5-fold; Fig. 2*C*). It is interesting that the larger aromatic moieties of flecainide project further toward the wall of the central cavity near the fenestrations compared with lidocaine, in light of the differences in physiological effects and pharmacological uses of these drugs. Flecainide and other class IC AADs bind to sodium channels more tightly and are used to treat atrial arrhythmias, whereas lidocaine and the class IB AADs dissociate more rapidly and are used to treat ventricular arrhythmias (*SI Appendix*, *SI Discussion*) (9). The difference in binding position that we observe in our crystal structures may underlie this therapeutically important difference in the off rate of binding and in clinical use. Overall, our results place the receptor site for these LA/AADs on the intracellular side of the selectivity filter in the central cavity in the pore of Na_VAb and reveal two overlapping, but distinct, binding poses for lidocaine and flecainide. However, higher-resolution images without fourfold averaging will be required to fully define the chemistry of drug binding for lidocaine.

Modifying the Size of the Fenestrations in Na_VAb. To probe the function of the fenestrations in providing drug access to the LA/AAD receptor site in the pore during resting-state drug block, we constructed the mutants Na_VAb/F203A and Na_VAb/F203W. Based on the capping position of the phenyl sidechain of F203 in the fenestrations of Na_VAb/WT (21), we expected these mutations to enlarge or restrict the fenestrations, respectively. Mutation of F203 to A or W had little or no effect on the conformation of Na_VAb or its S6 segments (Fig. 3 *A* and *B*). However, we found that Na_VAb/F203A has substantially wider fenestrations and that Na_VAb/F203W has more closed fenestrations compared with Na_VAb/WT (Fig. 3*C*). Two distinct rotamers were observed for the indole ring of W203, one of which blocked the fenestrations nearly completely (Fig. 3*C*). Analysis of solvent-accessible space in the fenestrations using the MOLE algorithm (Fig. 3*D*) revealed that the mutation F203A widens the fenestration at its narrowest point, whereas mutation F203W blocks solvent accessibility through the fenestration, primarily in its "down" rotamer conformation (Fig. 3*D* and *SI Appendix*, *SI Discussion*). These structural results confirm that these two mutations do indeed progressively change the size of the fenestrations, without other structural effects, and therefore are valid models for testing the effects of the size of the fenestrations on resting-state drug block.

Fenestration Size and Resting-State Block by Flecainide. In studies of drug block of mammalian Na_V channels, it is challenging to

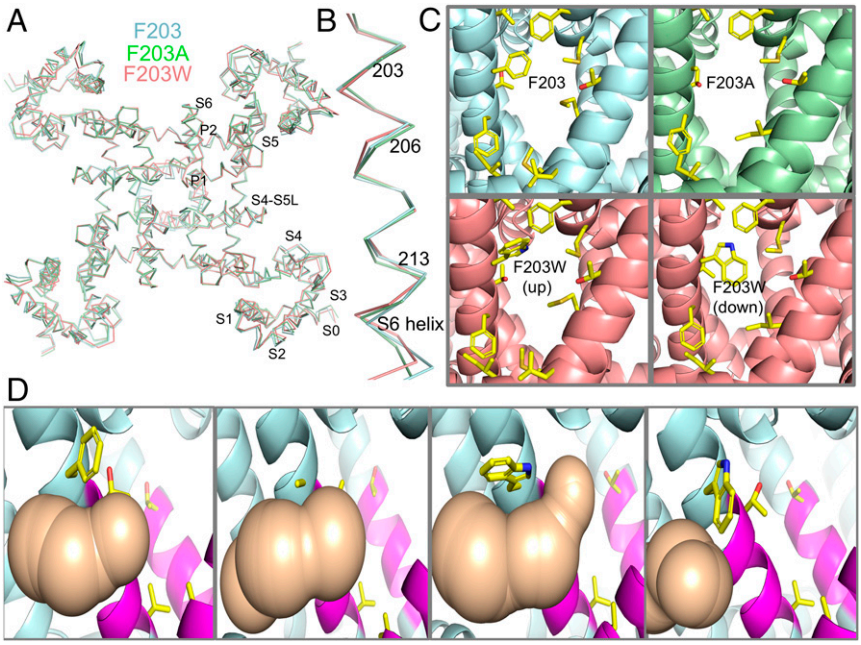

Fig. 3. Mutations of F203 alter the size of the fenestrations of Na_VAb. (*A*) Overlay of ribbon diagrams of Na_VAb/I217C (cyan), Na_VAb/I217C/F203A (green), and Na_VAb/I217C/F203W (salmon). (*B*) S6 segments displayed as in *A*. (*C*) The fenestration is shown in side view from the perspective of the membrane bilayer. The protein is displayed with cartoon representation of helices and select sidechains shown as sticks with the Na_VAb constructs indicated. Two rotamers ('up' and 'down') are shown for Na_VAb/I217C/F203W. (*D*) Analysis of solvent-accessible space in the fenestration (tan) computed by MOLE for the indicated Na_VAb constructs. Each fenestration and associated solvent-accessible space is shown in side view, but with 90° rotation around the vertical axis with respect to *C*.

definitively separate resting-state block from open-state block because the channel must be opened to assess its activity. However, in our initial studies of block of Na_vAb/WT by flecainide, we did not observe any frequency-dependent open-state block at pulse rates of 1, 10, and 20 Hz (Fig. 4 *A* and *B*). Thus, Na_VAb provides an ideal template for studies of resting-state drug block because there is little or no frequency-dependent block accumulating during test pulses. The lack of frequency-dependent block may result from the lack of the key F and Y residues (F1764 and Y1771 in $Na_V1.2$) that are required for frequency-dependent block (10), but are replaced by T206 and V213 in Na_VAb. Our experiments target the resting state of Na_VAb by allowing drug binding only at negative potentials at which these Na_VAb constructs are not detectably inactivated.

The F203A and F203W mutations significantly changed the voltage dependence of activation and inactivation of Na_VAb (*SI Appendix*, *SI Discussion*). To study resting-state block by flecainide specifically, Na_vAb/WT expressed in *Trichoplusia ni* cells was held at −140 or −160 mV, potentials that prevent inactivation of WT and mutant Na_VAb constructs, respectively (*SI Appendix*, *SI Discussion*, and Fig. S1). The cells were depolarized by 50-ms pulses in 10-mV steps ranging from −140 to +60 mV at 0.2 Hz. After collecting control data, flecainide was perfused over the cells for 2 min, and the amplitude of the peak sodium current during the first pulse after drug perfusion was taken as a measure of resting-state block. Fitting the concentration-response curve gave a Hill coefficient of 0.9 and an IC_{50} of 7 μM (Fig. 4*C*), comparable to the potency for block of mammalian Na_V channels (26, 27). If the main access pathway for resting-state block is through the fenestrations, changing their size should change the energy barrier for drug access in parallel. Mutating F203 to A, which makes the fenestrations wider (Fig. 3*C*), enhanced resting-state block by flecainide, reducing its IC_{50} to 0.9 μM (Fig. 4*C*). This corresponds to ∼7.7-fold higher potency compared with Na_vAb/WT. Conversely, the concentration-response curve for Na_vAb/F203W revealed an IC_{50} of 46 μM, an ∼6.5-fold lower potency compared with Na_vAb/WT (Fig. 4*C*). These results indicate that the size of the fenestrations affects access of flecainide to its receptor site in the pore by altering the size of the pathway for resting-state block, thereby modulating drug potency 51-fold when F203A is compared with F203W.

Effect of Fenestration Size on Resting-State Block by Lidocaine. Our electrophysiological and crystallographic data on interaction of flecainide with Na_VAb indicate that the size of the fenestrations is a critical factor that determines the level of resting-state block by LA/AADs. To further test that conclusion, we studied lidocaine, which has a smaller volume and polar surface area (PSA) than flecainide (V = 244.9 Å^3, PSA = 32.3 Å^2 vs. V = 331.9 Å^3, PSA = 59.6 Å^2). Concentration-response curves indicated an IC_{50} of 135 μM for the resting-state block of Na_vAb/WT (Fig. 5 *A* and *B*), similar to the bacterial Na_V channel NaChBac and mammalian cardiac Na_V channels (20, 28). Because the ratio of molecular volumes of lidocaine/flecainide is 0.7 and the PSA ratio is 0.54, we expected that the F203W mutation would shift the concentration-response curve to higher concentrations by ∼3.5- to 4.8-fold (*Materials and Methods*). Interestingly, we found that decreasing the size of the fenestrations in Na_vAb/F203W led to a 3.4-fold shift in the potency of resting-state block to higher concentrations (IC_{50} = 458 μM), which is in good agreement with our estimate based on the size of the drugs. On the other hand, expanding the size of the fenestration in Na_VAb/F203A did not increase resting-state block, indicating that the fenestrations of Na_VAb/WT are wide enough to pass lidocaine without any barrier and that increases in fenestration size therefore have no effect (Fig. 5*B*).

Effect of Fenestration Size on Resting-State Block by Benzocaine. If lidocaine has easy access through the fenestrations of NavAb/WT, a smaller drug should also give a similar resting-state block of Na_VAb/WT and Na_vAb/F203A. To examine that prediction, we measured resting-state block by benzocaine, the smallest LA with roughly half the size of flecainide (V = 157 Å^3 vs. V = 331.9 Å^3). We found no difference between the resting-state block of Na_VAb/WT and Na_VAb/F203A as expected (IC_{50} = 254 μM for Na_VAb/WT and IC_{50} = 279 μM Na_VAb/F203A) (Fig. 6 *A* and *B*). These results confirm that lidocaine's size is within the upper limit for accessing the fenestrations, and any smaller LA/AAD will diffuse easily without steric hindrance. The volume ratio of benzocaine compared with

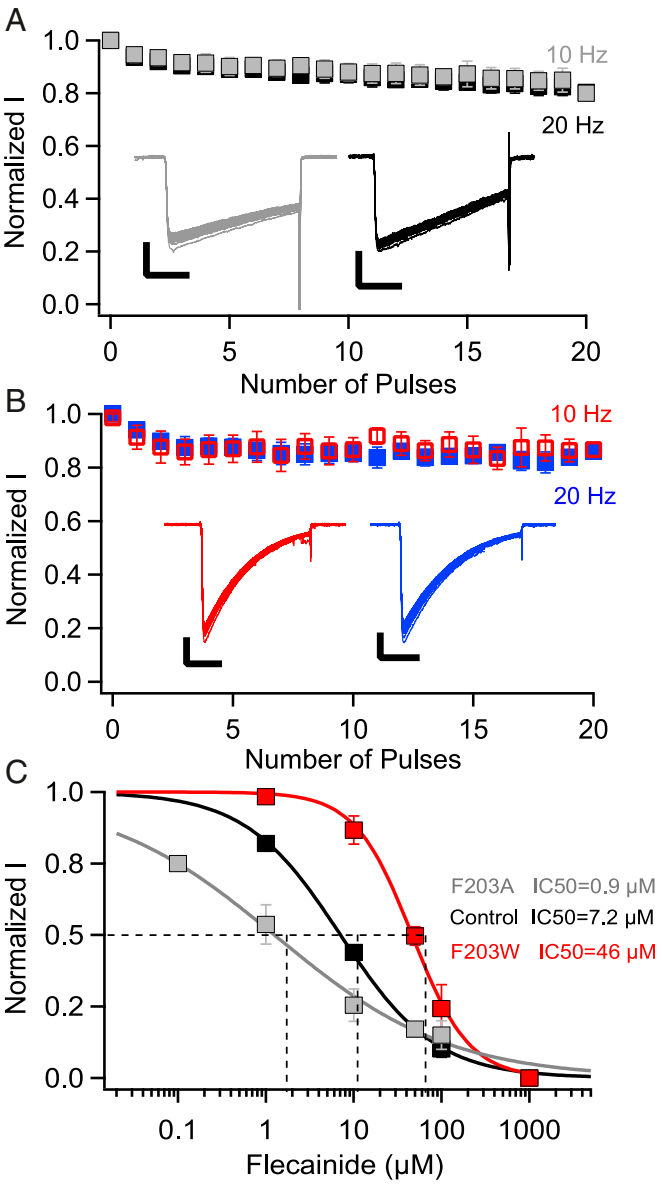

Fig. 4. Resting-state block of Na_VAb/WT, Na_VAb/F203A, and Na_VAb/F203W by flecainide. (*A*) Use-dependent inactivation of Na_vAb/WT in response to 30-ms repetitive pulses applied at 10 Hz (gray) or 20 Hz (black) from a holding potential of −160 mV to −20 mV. *Insets*, example sodium currents. (The vertical and horizontal scale bars represent 0.5 nA and 10 ms, respectively.) (*B*) Use-dependent block of Na_vAb/WT in response to 30-ms repetitive pulses applied at 10 Hz (red) or 20 Hz (blue) from a holding potential of −160 mV to −20 mV in the presence of 10 μM flecainide. *Insets*, example sodium currents. (The vertical and horizontal scale bars represent 0.5 nA and 10 ms, respectively.) (*C*) Concentration-response curves for flecainide inhibition of Na_vAb/WT (black, IC_{50} = 7.2 ± 0.4 μM), Na_vAb/F203W (red, IC_{50} = 46 ± 2 μM), and Na_VAb/F203A (gray, IC_{50} = 0.9 ± 0.01 μM).

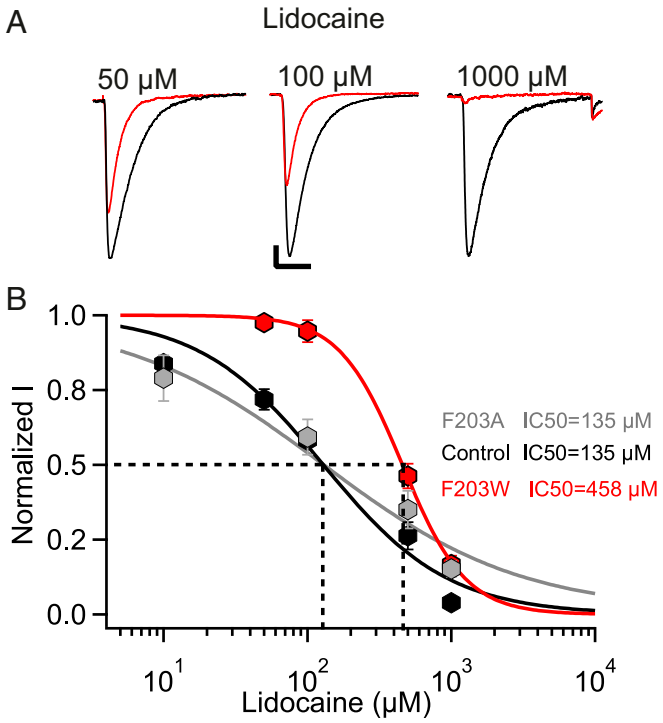

Fig. 5. Resting-state block of Na_VAb/WT, Na_VAb/F203W, and Na_VAb/F203A by lidocaine. (*A*) Sodium current recordings of Na_VAb/WT in the absence (black) and presence of the indicated concentrations of lidocaine (red). Current traces resulted from pulses applied from a holding potential of −160 mV to a test pulse = 0 mV. The vertical and horizontal scale bars represent 0.2 nA and 10 ms, respectively. (*B*) Concentration-response curves for lidocaine inhibition of Na_VAb/WT (black, IC_{50} = 135 ± 20 μM), Na_VAb/F203W (red, IC_{50} = 458 ± 9 μM), and Na_VAb/F203A (gray, IC_{50} = 135 ± 2 μM). Each data point is an average of 4–9 cells.

flecainide is 0.47. This difference in volume should result in an ∼3.1-fold positive shift in resting-state block of Na_VAb/F203W. Our results show an ∼2.6-fold shift in resting-state block by benzocaine compared with Na_VAb/WT (Na_VAb/F203W, IC_{50} = 739 μM; Na_VAb/WT, IC_{50} = 279 μM; Fig. 6 *A* and *B*), which fits our estimate of the effects of drug size.

Discussion

LAs and AADs Bind to a Receptor Site in the Central Cavity on the Intracellular Side of the Selectivity Filter. Our results reveal the binding sites for LAs and AADs in the central cavity of sodium channels. The positively charged amino groups of lidocaine and flecainide point toward the intracellular outlet of the ion selectivity filter into the central cavity, which is formed by the backbone carbonyl groups of T175 and therefore has a partial negative charge. This ionic interaction is crucial for LAs and AADs, which must be positively charged by protonation of their secondary or tertiary amino groups to be effective blockers (15). Our structures reveal important chemical interactions with T206, and the importance of this interaction was confirmed by site-directed mutagenesis. This amino acid residue is in the position of F1764 in mammalian sodium channels ($Na_V1.2$ numbering), which is also crucial for drug block (10, 11). In addition to these primary interactions, the aromatic rings of lidocaine and flecainide also make hydrophobic interactions with other amino acid residues lining the central cavity of Na_VAb that differ between the two drugs.

Unlike eukaryotic Na_V channels, Na_VAb and other bacterial Na_V channels are homotetramers (17) and have a nearly perfect fourfold symmetry in preopen and open states (21, 29). This symmetry presents a substantial obstacle to clear resolution of the structure of drugs bound at or near the central axis in the pore because four symmetrical binding poses are expected from averaging drug bound randomly to the four identical subunits across the many molecules in the crystal lattice. This expectation was clearly demonstrated in a previous study of a bacterial Na_V channel binding an experimental analgesic drug candidate containing a bromine (Br) atom in its aromatic ring (19). No electron density related to drug binding could be resolved because it was blurred by fourfold averaging of the signal, but four Br atoms could be discerned projecting toward the fenestrations from the central drug-binding site. Our results take an important step forward in analysis of drug binding at the LA/AAD receptor site in Na_V channels by revealing drug-dependent electron density for clinically used drugs and by providing insights into the different poses for LA and AAD binding to this receptor site. However, studies of human sodium channels with drugs bound will be required to fully define this clinically important receptor site (*SI Appendix*, *SI Discussion*).

Fenestrations Control Resting-State Block. Changes in the size of the fenestrations caused by mutations, without any change in the local conformation of the pore, cause large, predictable increases or decreases in resting-state block. These results implicate drug passage through the fenestrations as a primary determinant of resting-state block, and they elucidate the long-sought molecular mechanism for direct drug entry from the membrane phase to the lumen of the pore, as originally proposed in the Modulated Receptor Hypothesis (15, 16) and in the related Guarded Receptor

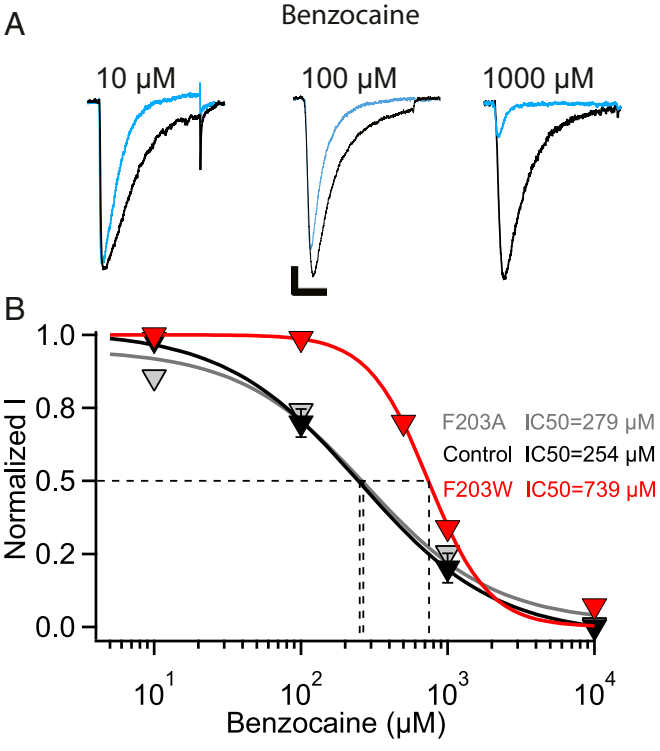

Fig. 6. Resting-state block of Na_VAb/WT, Na_VAb/F203W, and Na_VAb/F203A by benzocaine. (*A*) Sodium current recordings of Na_VAb/WT in the absence (black) and presence of the indicated concentrations of benzocaine (blue). Current traces resulted from pulses applied from a holding potential of −160 mV to a test pulse of 0 mV. The vertical and horizontal scale bars represent 0.5 nA and 10 ms, respectively. (*B*) Concentration-response curves for benzocaine inhibition of Na_VAb/WT (black, IC_{50} = 254 ± 37 μM), Na_VAb/F203W (red, IC_{50} = 739 ± 38 μM), and Na_VAb/F203A (gray, IC_{50} = 279 ± 3 μM), bottom. Each data point is an average of 4–9 cells.

Hypothesis (30). LAs and AADs are secondary or tertiary amines, which are thought to pass through the membrane in uncharged form and then reprotonate before binding (*SI Appendix*, *SI Discussion*) (15, 16). In the context of the Modulated Receptor Hypothesis (15), voltage-dependent tonic block is determined by direct drug access through the fenestrations, binding to the drug receptor site, and voltage-dependent conformational change to the high-affinity drug-bound inactivated state. In contrast, frequency-dependent block is determined by the ratio of the phasic rate of drug access through repetitive opening of the activation gate to the continuous tonic rate of drug access through the fenestrations. These state-dependent forms of drug block are crucial for clinical use of Na_V-channel–blocking drugs for local anesthesia, cardiac arrhythmia, epilepsy, and chronic pain.

The differences in the binding poses and in the effects of the size of the fenestrations on block by flecainide (a class IC AAD) and lidocaine (a class IB AAD) that we have observed are particularly important because these two drug classes have complementary uses in treatment of atrial vs. ventricular arrhythmias, respectively (*SI Appendix*, *SI Discussion*) (9). Our results suggest that both differences in the binding poses of lidocaine and flecainide at their receptor site and differences in the kinetics of drug interaction with the LA/AAD receptor site that are controlled by the fenestrations may contribute to this crucial difference in the clinical use of these widely prescribed AADs.

Fenestrations and Structure-Based Drug Design. Our results introduce an unprecedented concept into rational drug design by showing that future structure-based design of LA/AADs, next-generation analgesics and antiepileptics, and other pore blockers of Na_V channels should consider the size and conformations of the fenestrations in resting and activated/inactivated states of Na_V channels in addition to the chemical features of the drug receptor site. In this respect, it has been shown that lidocaine and other AADs have differential potencies for block of the different isoforms of mammalian Na_V channels in the resting state (31). Part of this differential blocking activity may be caused by differences in fenestration size. As a result, recovery from LA/AAD inhibition likely varies between different Na_V channel isoforms, further emphasizing the importance of an isoform-specific rational drug design that includes effects of the architecture of the fenestrations. The discovery of disease mutations that cause arrhythmias by altering amino acid residues that line the fenestrations of $Na_v1.5$ indicates that individual genetic variation may also influence drug access through the fenestrations for resting-state block (32). Evidently, choice of the right drug that would be effective in treating specific arrhythmias will depend on the amino acid signature of the fenestrations in addition to the amino acid residues that contribute to the drug receptor site itself. Recent studies extend the discovery of fenestrations to potassium channels and reveal drug binding to the fenestrations themselves (*SI Appendix*, *SI Discussion*) (25). These studies suggest that fenestrations may have pharmacological significance for other major classes of ion channels in addition to voltage-gated sodium channels.

Materials and Methods

The Na_VAb channel and mutants were expressed in *T. ni* cells, solubilized, purified, and crystallized, and their structures were determined by X-ray crystallography as described previously (22, 29). The functional properties of Na_VAb and mutants were determined by expression in *T. ni* cells and whole-cell voltage clamp analysis as described previously (33). See *SI Appendix*, *SI Materials and Methods*, for details.

ACKNOWLEDGMENTS. We thank the beamline staff at the Advanced Light Source (BL8.2.1 and BL8.2.2) for their assistance during data collection and Dr. Jin Li for assistance in molecular biology and manuscript preparation. This research was supported by Research Grant R01 NS15751 from the National Institutes of Health (NIH) (to W.A.C.); by Research Grant R01 HL112808 from the NIH (to W.A.C. and N.Z.); and by the Howard Hughes Medical Institute (N.Z.).

1. Hille B (2001) *Ionic Channels of Excitable Membranes* (Sinauer Associates Inc., Sunderland, MA), 3rd Ed.
2. Catterall WA (2000) From ionic currents to molecular mechanisms: The structure and function of voltage-gated sodium channels. *Neuron* 26:13–25.
3. Catterall WA, Zheng N (2015) Deciphering voltage-gated Na^+ and Ca^{2+} channels by studying prokaryotic ancestors. *Trends Biochem Sci* 40:526–534.
4. Catterall WA (2014) Sodium channels, inherited epilepsy, and antiepileptic drugs. *Annu Rev Pharmacol Toxicol* 54:317–338.
5. Dib-Hajj SD, Cummins TR, Black JA, Waxman SG (2010) Sodium channels in normal and pathological pain. *Annu Rev Neurosci* 33:325–347.
6. Venance SL, et al.; CINCH investigators (2006) The primary periodic paralyses: Diagnosis, pathogenesis and treatment. *Brain* 129:8–17.
7. Clancy CE, Kass RS (2002) Defective cardiac ion channels: From mutations to clinical syndromes. *J Clin Invest* 110:1075–1077.
8. Butterworth JFI, IV, Strichartz GR (1990) Molecular mechanisms of local anesthesia: A review. *Anesthesiology* 72:711–734.
9. Sampson KJ, Kass RS (2011) Antiarrhythmic drugs. Goodman & Gilman's Pharmacological Basis of Therapeutics, eds L. Brunton, B. Chabner, B. Knollman (McGraw-Hill, New York), 12th Ed, pp 815–848.
10. Ragsdale DS, McPhee JC, Scheuer T, Catterall WA (1994) Molecular determinants of state-dependent block of Na^+ channels by local anesthetics. *Science* 265:1724–1728.
11. Ragsdale DS, McPhee JC, Scheuer T, Catterall WA (1996) Common molecular determinants of local anesthetic, antiarrhythmic, and anticonvulsant block of voltage-gated Na^+ channels. *Proc Natl Acad Sci USA* 93:9270–9275.
12. Yarov-Yarovoy V, et al. (2001) Molecular determinants of voltage-dependent gating and binding of pore-blocking drugs in transmembrane segment IIIS6 of the Na^+ channel alpha subunit. *J Biol Chem* 276:20–27.
13. Yarov-Yarovoy V, et al. (2002) Role of amino acid residues in transmembrane segments IS6 and IIS6 of the Na^+ channel alpha subunit in voltage-dependent gating and drug block. *J Biol Chem* 277:35393–35401.
14. Pless SA, Galpin JD, Frankel A, Ahern CA (2011) Molecular basis for class Ib antiarrhythmic inhibition of cardiac sodium channels. *Nat Commun* 2:351.
15. Hille B (1977) Local anesthetics: Hydrophilic and hydrophobic pathways for the drug-receptor reaction. *J Gen Physiol* 69:497–515.
16. Hondeghem LM, Katzung BG (1984) Antiarrhythmic agents: The modulated receptor mechanism of action of sodium and calcium channel-blocking drugs. *Annu Rev Pharmacol Toxicol* 24:387–423.
17. Ren D, et al. (2001) A prokaryotic voltage-gated sodium channel. *Science* 294: 2372–2375.
18. Boiteux C, et al. (2014) Local anesthetic and antiepileptic drug access and binding to a bacterial voltage-gated sodium channel. *Proc Natl Acad Sci USA* 111:13057–13062.
19. Bagnéris C, et al. (2014) Prokaryotic NavMs channel as a structural and functional model for eukaryotic sodium channel antagonism. *Proc Natl Acad Sci USA* 111: 8428–8433.
20. Lee S, Goodchild SJ, Ahern CA (2012) Local anesthetic inhibition of a bacterial sodium channel. *J Gen Physiol* 139:507–516.
21. Payandeh J, Scheuer T, Zheng N, Catterall WA (2011) The crystal structure of a voltage-gated sodium channel. *Nature* 475:353–358.
22. Payandeh J, Gamal El-Din TM, Scheuer T, Zheng N, Catterall WA (2012) Crystal structure of a voltage-gated sodium channel in two potentially inactivated states. *Nature* 486:135–139.
23. Shen H, et al. (2017) Structure of a eukaryotic voltage-gated sodium channel at near-atomic resolution. *Science* 355:eaal4326.
24. Yan Z, et al. (2017) Structure of the Nav1.4-β1 complex from electric eel. *Cell* 170: 470–482.e11.
25. Wrobel E, et al. (2016) KCNE1 induces fenestration in the Kv7.1/KCNE1 channel complex that allows for highly specific pharmacological targeting. *Nat Commun* 7: 12795.
26. Liu H, Atkins J, Kass RS (2003) Common molecular determinants of flecainide and lidocaine block of heart Na^+ channels: Evidence from experiments with neutral and quaternary flecainide analogues. *J Gen Physiol* 121:199–214.
27. Ramos E, O'Leary ME (2004) State-dependent trapping of flecainide in the cardiac sodium channel. *J Physiol* 560:37–49.
28. Bean BP, Cohen CJ, Tsien RW (1983) Lidocaine block of cardiac sodium channels. *J Gen Physiol* 81:613–642.
29. Lenaeus MJ, et al. (2017) Structures of closed and open states of a voltage-gated sodium channel. *Proc Natl Acad Sci USA* 114:E3051–E3060.
30. Starmer CF, Grant AO, Strauss HC (1984) Mechanisms of use-dependent block of sodium channels in excitable membranes by local anesthetics. *Biophys J* 46:15–27.
31. Sheets PL, Heers C, Stoehr T, Cummins TR (2008) Differential block of sensory neuronal voltage-gated sodium channels by lacosamide [(2R)-2-(acetylamino)-N-benzyl-3-methoxypropanamide], lidocaine, and carbamazepine. *J Pharmacol Exp Ther* 326: 89–99.
32. Huang W, Liu M, Yan SF, Yan N (2017) Structure-based assessment of disease-related mutations in human voltage-gated sodium channels. *Protein Cell* 8:401–438.
33. Gamal El-Din TM, Martinez GQ, Payandeh J, Scheuer T, Catterall WA (2013) A gating charge interaction required for late slow inactivation of the bacterial sodium channel NavAb. *J Gen Physiol* 142:181–190.